Supplementary information

Oxidation Under Air of Tavorite $LiVPO_4F$: Influence of Vanadyl-type Defects on its Electrochemical Properties

Edouard Boivin [a, b, f], Jean-Noël Chotard [b, f, g], Michel Ménétrier [a, f], Lydie Bourgeois [c, d], Tahya Bamine [a, f], Dany Carlier [a, f], François Fauth [e], Christian Masquelier [b, f, g] and Laurence Croguennec [a, f, g,*]

[a] *CNRS, Univ. Bordeaux, Bordeaux INP, ICMCB UPR 9048, F-33600 Pessac, France.*

[b] *Laboratoire de Réactivité et de Chimie des Solides, CNRS-UMR#7314, Université de Picardie Jules Verne, F-80039 Amiens Cedex 1, France.*

[c] *Université de Bordeaux, ISM, Groupe de Spectroscopie Moléculaire, F-33405 Talence, France.*

[d] *Bordeaux INP, ISM, CNRS, UMR 5255, F-33405, Talence, France.*

[e] *CELLS - ALBA synchrotron, E-08290 Cerdanyola del Vallès, Barcelona, Spain.*

[f] *RS2E, Réseau Français sur le Stockage Electrochimique de l'Energie, FR CNRS 3459, F-80039 Amiens Cedex 1, France.*

[g] *ALISTORE-ERI European Research Institute, FR CNRS 3104, F-80039 Amiens Cedex 1, France.*

Figure S1: *Comparison of Raman and CHNS results. Square symbol: Raman intensity of LVPF-T carbon signals integrated between 1200 and 1700 cm^{-1} normalized by the one of LVPF. Circle symbol: Carbon content of LVPF-T samples obtained by CHNS normalized by the one of LVPF. In inset, Raman spectra of LVPF and LVPF-375 in the 1200 - 1700 cm^{-1} region showing better-resolved signals assigned to carbon contribution at high annealing temperature.*

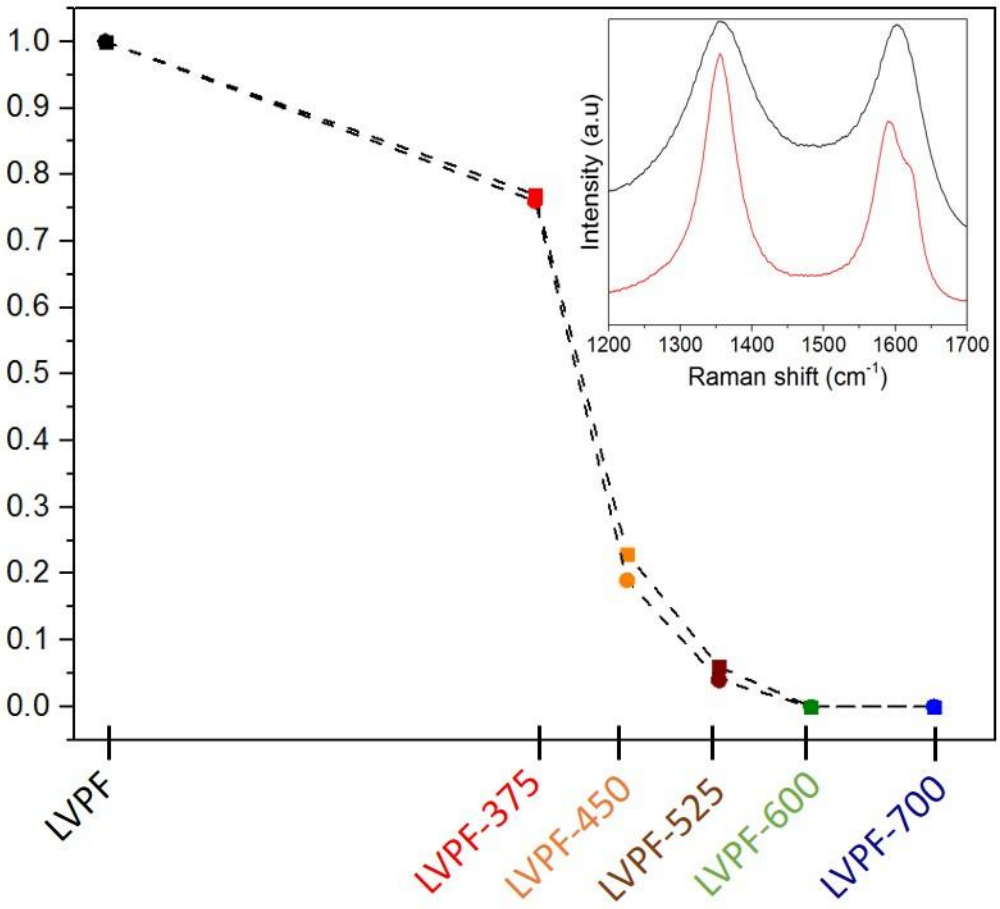

Raman scattering measurements were performed with a Horiba Jobin Yvon Labram HR-800 micro-spectrometer. Spectra were recorded with a 514.5 nm excitation wavelength of an Ar^+ laser, with a power adjusted to ca. 50 µW in order to avoid any degradation of the sample. Raman spectra shown in **Figure S1** are characteristic of each material and extracted from mapping on pellet surfaces of about 1000 µm² (samples were previously pressed in pellets in order to analyze a flat surface). Raman signals observed in the 1200-1700 cm^{-1} range

correspond to the carbon contribution. The 1580 cm^{-1} band is assigned to sp^2-hybridized carbons systems (G line, Raman-allowed E_{2g} mode in the ideal graphite). The 1380 cm^{-1} band corresponds to a disorder-induced line (D line) due to the presence of structural defects, as well as the weak 1620 cm^{-1} band (D' line), observed for the better-resolved spectra at high annealing temperature [1]. The evolution of the integrated intensity of these carbon signals is related to the one of the carbon amount. Raman measurements reveal a strong decrease of the carbon content with the increase of the annealing temperature, but also the presence of residual carbon until 525°C, in agreement with CHNS results.

Figure S2: *evolution of cell parameters (a, triangle, b, square and c, circle) of the LVPF, LVPF-375, LVPF-450, LVPF-525, LVPF-600, LVPF-700, LVPO and single crystals from [2] (empty marks) as function of the average oxidation state of Vanadium.*

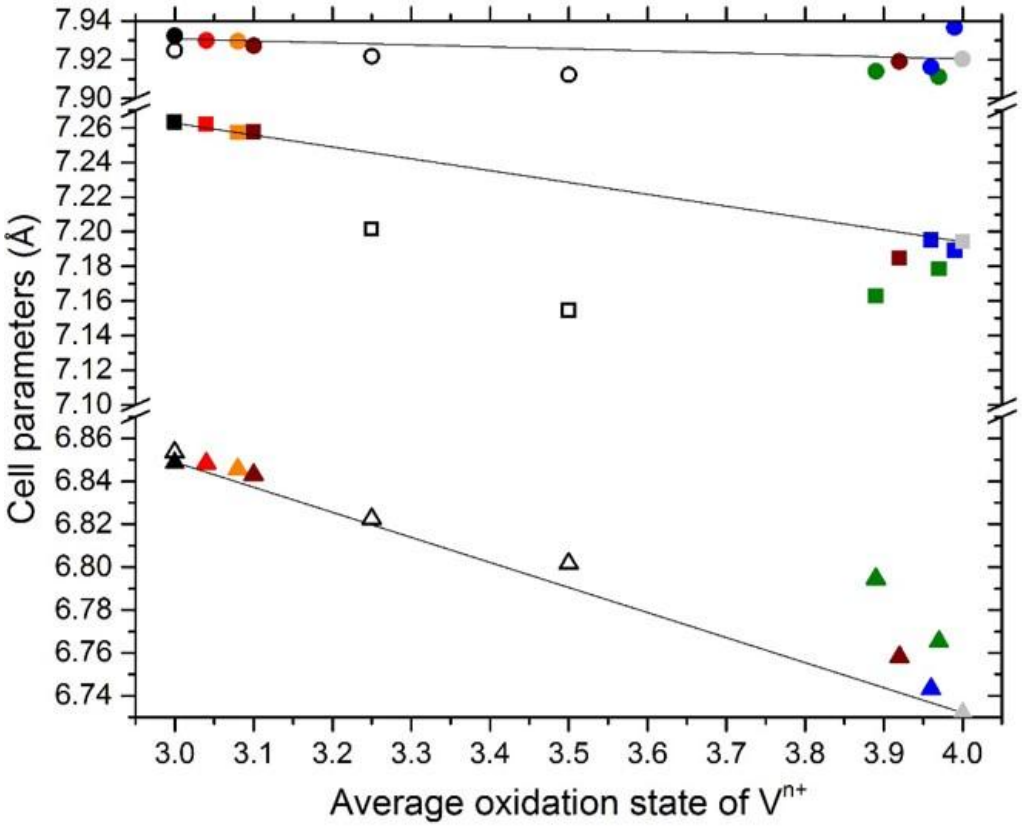

The Rietveld refinements of all the samples discussed in this article lead to the determination of their cell parameters: it was shown that they do not follow the Vegard's law, it is especially true for the a and b parameters. A previous work studying the structure of single crystals showing the compositions $LiVPO_4F_{1-x}O_x$ (with x = 0, x = 0.29 and x = 0.53) reports similar results, *i.e.* cell parameters which do not follow the Vegard's law on the contrary to the cell volume[2]. Our hypothesis is that the "solubility" of the V-F and vanadyl (V=O) bonds along the chains is not easy. Indeed, the cell parameter which reveals the larger gap to the Vegard's law is b, which corresponds to the propagation direction of the chains.

Table S1: Experimental and calculated NMR shifts for two lithium and two phosphorus sites in $LiVPO_4O$ using GGA, GGA+U (with U= 3.5 eV) and GGA/hybrid computational models[3]

$LiVPO_4O$	shift exp.	GGA	GGA+U	GGA/hyb
Li(1)	79	98	58	103
Li(2)	79	95	52	95
P(1)	1593	2990	1810	2170
P(2)	1418	2630	1533	1849

Figure S3: *^{19}F normalized (according to the mass of the sample) NMR spectra of LVPF, LVPF-375, LVPF-450, LVPF-525, LVPF-600, LVPF-700, and LVPO. In inset, zooms of the isotropic signals associated to the different contributions. The isotropic peaks are noted by #, their spinning side bands by * and additional contributions by ∇.*

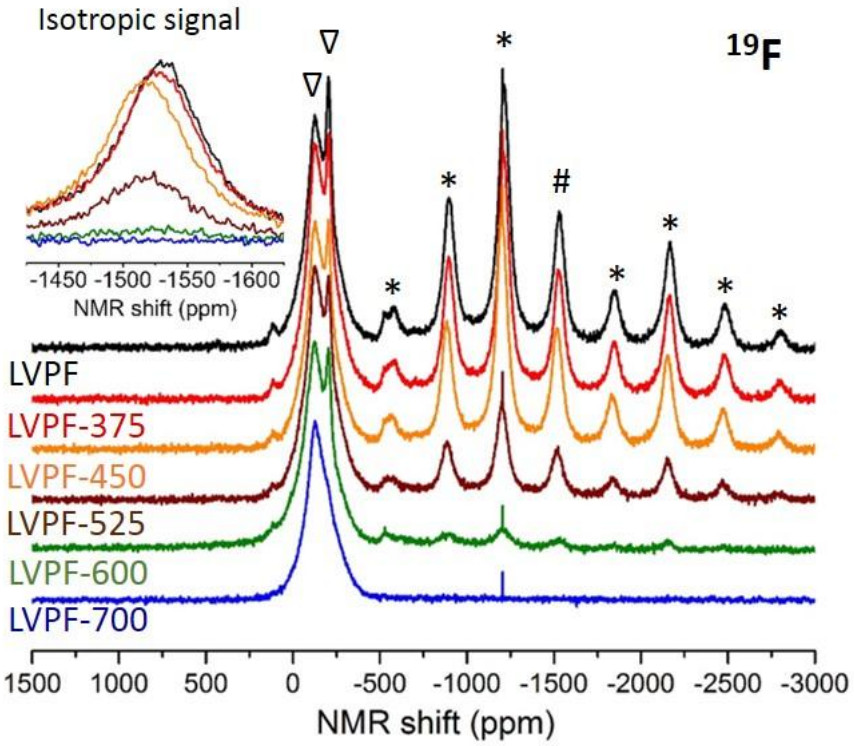

^{19}F MAS NMR spectrum of LVPF exhibits a strong parasitic contribution from the probe (which contains Teflon) around 150 ppm, and a non-shifted signal assigned to residual LiF. The isotropic peak is located at -1500 ppm. All others signals are assigned to spinning side bands. From 375°C, the global intensity of the signal decreases gradually until 700°C due to the replacement of oxygen for fluorine. Nevertheless, surprisingly, no others peaks which would be assigned to Fluorine atom in interaction with a V^{4+} can be detected. The strong V-F interaction would lead to the appearance of very broad signal hardly discernible to the background. Moreover, the high number of spinning sidebands coupled to the narrow solid solution domain and the noisy signal obtained could hide the appearance of the contributions expected. Furthermore, the intensity of the non-shifted signal assigned to LiF decreases gradually with the temperature whereas ^{7}Li MAS NMR suggests an increasing amount of the diamagnetic phase(s). LiF is also affected by the

annealing and probably react with water contained in air to form LiOH and HF. Indeed, ^{1}H MAS NMR experiments were performed and highlight an increasing diamagnetic signal with the increasing temperature, which can be assigned to LiOH signature.

***Figure S4**:* Galvanostatic curves obtained versus Lithium at a C/50 rate for all the annealed samples: (a) in the high voltage domain (*i.e.* between 3.0 and 4.6 V *vs* Li^+/Li) and (c) in the low voltage domain (1.5 - 3.0 V *vs* Li^+/Li). The corresponding derivative curves are given in (b) and (d). The evolution of the discharge capacity at C/10 is given in inset of (a).

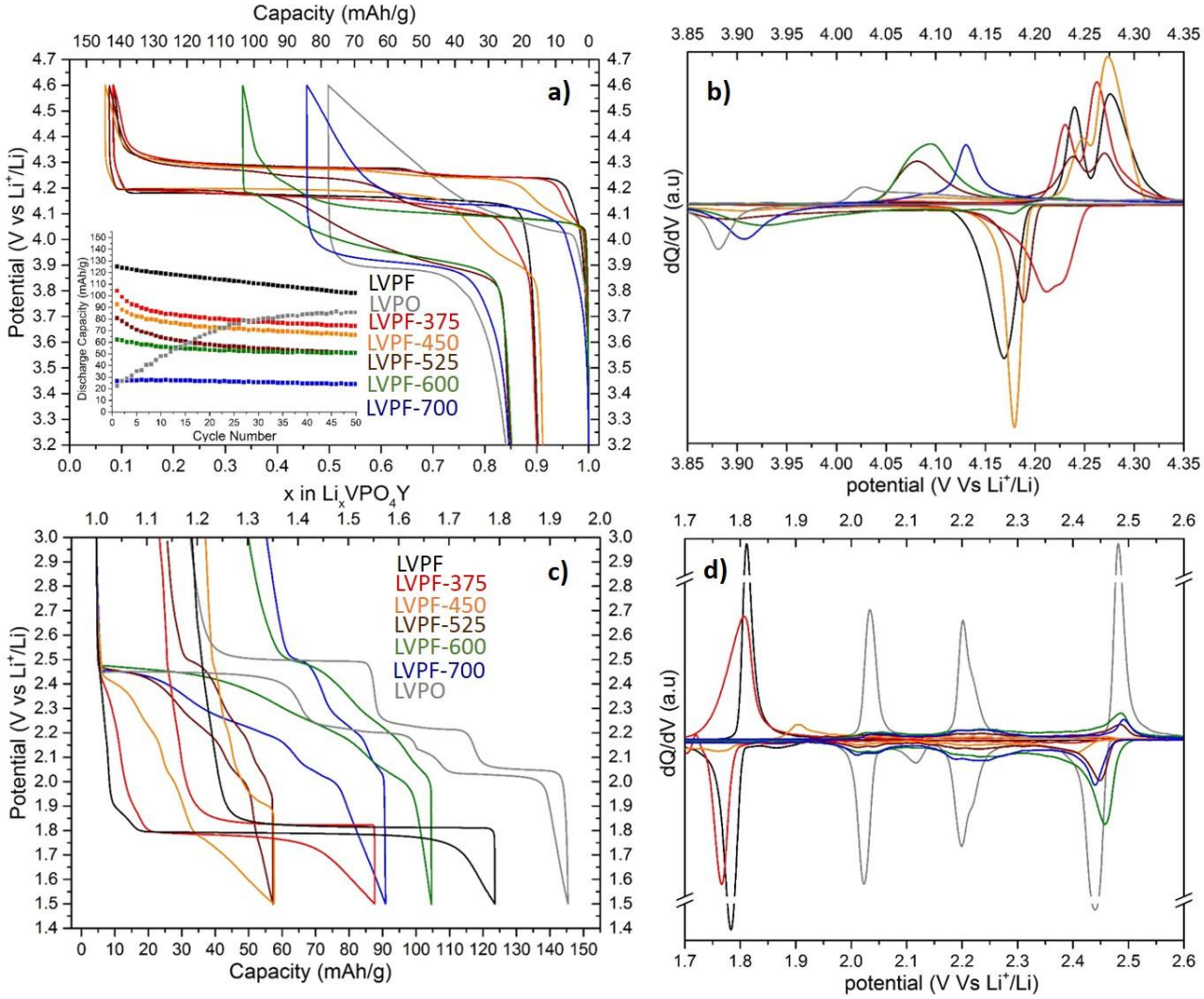

Figure to be included in the text as a double columns figure

Table S2: *comparison of the results obtained in this work with those obtained by Ma et al. in [4]*

	This work	**Ma *et al.*** [4]
Chemical analysis	1Li:1V:1P	(1-x)Li:1V:1P (with $0 \leq x \leq 0.2$)
TGA-MS	Loss of 6wt% (C → CO_2) at 450°C Loss of 1.7wt% (F → HF) at 525°C	Loss of 7,14wt% (C → CO_2 + F → ?) at 450°C
XRD	Pure pristine material Good Rietveld refinement based on high Resolution Synchrotron data considering anisotropic strains model $LiVPO_4F_{1-\varepsilon}O_\varepsilon$ + $LiVPO_4F_{\varepsilon'}O_{1-\varepsilon'}$ with $\varepsilon, \varepsilon' < 0.1$	$Li_3V_2(PO_4)_3$ impurity as revealed by Laboratory X-ray diffraction pattern (CuKα radiation) No cell parameters reported, whereas they are expected to be sensitive to a change in composition Single phases $Li_{1-x}VPO_4F_{1-y}O_y$ with $0 \leq x \leq 0.2$ and $0.1 \leq y \leq 0.9$
MEB	Sintering + carbon disappearance	Sintering + carbon disappearance
XPS	-	Fluorine deficiency (0.38 instead of 1) No fluorine seen on the surface at 550°C
IR	Appearance and shift of V=O Appearance of PO_4 ($LiVPO_4O$-type) Appearance of H-O-H	Appearance of V=O Appearance of PO_4 ($LiVPO_4O$-type) Appearance of H-O-H
Electrochemistry	No $Li_3V_2(PO_4)_3$ impurity A plateau appears at 4V at increasing T whereas that at 4.2V disappears Gradual decrease in capacity with increasing T	$Li_3V_2(PO_4)_3$ impurity A plateau appears at 4V at increasing T whereas that at 4.2V disappears Drastic drop in capacity at 550°C
NMR	Defects in the pristine material Appearance of a series of signals (LVPO-type with O—V^{IV}=O, and others intermediates)	-

(1) Ferrari, A. C.; Basko, D. M. Raman Spectroscopy as a Versatile Tool for Studying the Properties of Graphene. *Nat. Nanotechnol.* **2013**, *8*, 235–246.

(2) Onoda, M.; Ishibashi, T. Phase Transition and Spin Dynamics of the LiVFPO 4 Insertion Electrode with the S = 1 Linear Chain and the Development of F – O Mixed System. **2015**, *044802*, 1–5.

(3) Zhang, Y.; Castets, A.; Carlier, D.; Me, M. Simulation of NMR Fermi Contact Shifts for Lithium Battery Materials : The Need for an E Ffi Cient Hybrid Functional Approach. *J. Phys. Chem. C* **2012**, *116*, 17393–17402.

(4) Ma, R.; Shao, L.; Wu, K.; Shui, M.; Wang, D.; Long, N.; Ren, Y.; Shu, J. Effects of Oxidation on Structure and Performance of LiVPO4F as Cathode Material for Lithium-Ion Batteries. *J. Power Sources* **2014**, *248*, 874–885.